Graphene oxide-modified cellulose acetate membranes with improved Congo red removal efficiency

Mosa Jafer[1] (ORCID ID: 0009-0009-4557-5522), **Hayder Ali Mindeel**[1] (0009-0002-8198-3733), **Abdullah A. Hussein**[2] (0009-0006-6621-8581), **Naeemah A. Ibrahim**[3, *] (0009-0000-1012-5438), **Anmar Ghanim Taki**[4] (0009-0006-1262-9764), **Maadh Fawzi Nassar**[5, 6, *] (0000-0002-1610-0538)

DOI: https://doi.org/10.14314/polimery.2024.10.3

Abstract: The casting method was used to obtain membranes from cellulose acetate (CA) with different contents (0.1; 0.4; 0.8 wt%) of graphene oxide (GO). FESEM and FT-IR were used to evaluate the membrane structure. The contact angle was also examined. Congo red was used to evaluate the membrane efficiency. The contact angle of CA/GO membranes decreased from 55.47° (CA) to 38.16° (0.4 wt% GO), which indicates good dispersion of GO in the CA matrix. CA/GO membranes showed less irreversible fouling, which indicates that reversible fouling predominated over fouling of all membranes. Increasing the membrane porosity, pore size and hydrophilicity results in higher permeability.

Keywords: water treatment, graphene oxide, membranes, cellulose acetate.

Membrany z octanu celulozy modyfikowanego tlenkiem grafenu o poprawionej skuteczności usuwania czerwieni Kongo

Streszczenie: Metodą odlewania otrzymano z octanu celulozy (CA) membrany różniące się zawartością (0,1; 0,4; 0,8% mas.) tlenku grafenu (GO). Do oceny struktury membran zastosowano FESEM i FT-IR. Zbadano również kąt zwilżania. Czerwieni Kongo użyto do oceny wydajności membrany. Kąt zwilżania membran CA/GO zmniejszył się z 55,47° (CA) do 38,16° (0.4% mas. GO), co świadczy o dobrej dyspersji GO w osnowie CA. Membrany CA/GO wykazywały mniejsze nieodwracalne zanieczyszczenie, co wskazuje, że odwracalne zanieczyszczenie przeważało nad zanieczyszczeniem wszystkich membran. Zwiększenie porowatości membran, wielkości porów i ich hydrofilowości skutkuje większą przepuszczalnością.

Słowa kluczowe: uzdatnianie wody, tlenek grafenu, membrany, octan celulozy.

Filtration membranes are often made of two-dimensional (2D) materials that have a high aspect ratio, favorable dimensional selection properties, and remarkable chemical stability [1]. Graphene oxide (GO) is characterized by its good mechanical strength, chemical stability, chemical adaptability, and user-friendly size control qualities [2, 3]. GO is one substance that is frequently utilized in the production of membranes [4]. Water desalination [5], dye removal [6], oil–water separation [7], gas separations [8], luminescence [9], and electrochemical applications [10] are just a few of the many uses for GO-containing membranes that have been proposed. If pore diameters can be regulated via perforation, intercalated layers, and composite membranes, graphene materials can be employed as molecular sieves [11].

The attributes of high-performance membranes—elevated flux, superior rejection, robust mechanical strength, enhanced fouling resistance, and exceptional stability in aquatic environments—render them ideal for water purification [12]. Graphene oxide membranes exhibit restricted flow and inadequate structural stability, although they provide favorable ion selectivity [13]. Robust interactions, such as chemical cross-linking, might enhance stability; yet the water permeability of dense GO membranes is considerably affected by these alterations. Conversely, GO membranes exhibiting weak

[1] Ministry of Education, Al-Karkh district, Baghdad10001, Iraq.

[2] Polymer Research Center, University of Basrah, Basrah 61004, Iraq.

[3] Southern Technical University, Basrah 61004, Iraq.

[4] Department of Radiology Techniques, health and medical techniques college, Alnoor University, Mosul, Iraq.

[5] Integrated Chemical BioPhysics Research, Faculty of Science, Universiti Putra Malaysia, 43400 UPM Serdang, Selangor, Malaysia.

[6] Department of Chemistry, Faculty of Science, Universiti Putra Malaysia, 43400 UPM Serdang, Selangor, Malaysia.

[*] Authors for correspondence: naeema.ibrahim@stu.edu.iq, nassarmaadh@gmail.com

and stable hydrophobic or π–π interactions may lack the robustness necessary to endure actual water filtration procedures [14]. It is therefore rational to integrate GO with polymer carriers to create GO-based composite membranes [15]. These techniques can enhance the mechanical robustness and screening effectiveness of the GO membrane while concurrently enhancing water flux.

Graphene oxide membranes provide high permeance and effective separation capabilities. Huang and colleagues discovered that ionic sieving was improved by reduced GO membranes [11]. Manobalan *et al*. corroborated the previous observation, reporting a water permeance of 200 L/m^2×h×bar and over 80% rejection of 1M sodium chloride. Furthermore, hybrid GO/graphene multilayer membranes were employed to extract ionic dyes with an efficiency above 96% from an aqueous solution [16]. According to Azadi *et al*. [17], it demonstrated remarkable performance (> 99.9%) for analogous dye removal in organic solvent nanofiltration (OSN). Despite the promising results in the removal of ionic contaminants, challenges persist. The removal of dissolved natural organic matter (NOM) is typically a significant challenge in municipal water treatment. Extracting NOMs from water is challenging due to their hydrophilic and hydrophobic components. Congo Red is the principal component of natural organic matter (NOM) among several other chemicals [18]. Congo Red is considered a complex compound consisting of molecules with dimensions between 1.2 nm (12 Å). The typical molecular diameter of Congo Red is around 400 nm, with most molecules exceeding 5 nm in size [19]. To enhance dye removal efficacy using GO membranes in industrial applications, it is essential to identify the optimal balance between membrane permeance and rejection, both of which are closely related to membrane thickness. Graphene oxide (GO) nanosheets have gained attention as promising materials for high-performance separation membranes due to their remarkable chemical stability and ultrathin structure. Notably, GO membranes assembled from 2D nanosheets offer significant advantages in molecular and ionic sieving because of their efficient mass transfer, separation capabilities, and unique 2D transport channel structure [20–23]. With careful design and fabrication, GO membrane structures have the potential to achieve precise molecule and ion separation. However, the use of pure GO membranes in acidic environments can compromise their structure, limiting their effectiveness in ionic sieving [24–26]. To enhance the ionic separation performance and structural stability of GO membranes, reduction and cross-linking techniques are employed. Thebo and colleagues developed a type of reduced GO membrane with increased interlayer spacing by using tannic acid (TA) and theanine amino acid (TH) as cross-linkers and reducing agents [27, 28]. These GO composite membranes demonstrated exceptional structural stability, even after being immersed in water for 30 days, across a range of pH values. Such methods help control the lamellar spacing and charge of GO membranes, while also improving their mechanical strength by enhancing the attraction between GO nanosheets. For selective separation of mono- and multivalent metal cations, GO membranes often rely on size sieving and charge repulsion mechanisms [29–31].

In this paper, a procedure for water purification using GO-modified CA was developed. Congo red (feed concentration 500 mg/L) was removed from the membrane to an average flux of 7.75 (L/cm^2×h) under filtration pressure (6 bar). A comprehensive analysis of the influence of GO content on the filtration efficiency of CA-based membranes was also presented. Therefore, this work may provide an opportunity for industrial removal of organic water waste based on GO membranes.

EXPERIMENTAL PART

Materials

Aceton was acquired from Merck (Rahway, NJ, USA), while cellulose acetate (CA) was bought from GoodFellow (Huntington, England). Graphene oxide and Congo Red dye was acquired form Sigma Aldrich (St. Louis, MO, USA).

Methods

Synthesis of CA/GO membranes

Using the PHILOS flat sheet membrane casting technology (Gwangmyeong-si, South Korea), phase inversion technique was utilized to create all the membranes used in this study. Different loadings of GO (0.1, 0.4, and 0.8 wt%) in the dope 10 wt% CA in acetone (1:10) solutions were used to generate GO/CA membrane samples. Initially, the CA and GO were dried for two hours at 50°C in an oven. After that, CA and GO were separately dissolved in 100% acetone for six hours at 40°C whiles being constantly stirred. For sixty minutes, both solutions were subjected to ultrasonication (Wildstir WUC. D06H, Daihan Scientific, Seoul, South Korea). The solutions were then combined while being stirred at 600 rpm for two hours at room temperature. After that, an ultrasonic degasser was used for sixty minutes. The combination was then cast, at room temperature, using a casting knife with a gap height of approximately 150 μm and a casting speed of 1.5 m/min on the surface of a clean glass plate. Following casting, the thin film coated glass plate was submerged in room temperature (25°C) deionized water (DW) and left there until the membrane fully peeled off the plate (overnight). To get rid of all solvent residue, the manufactured membranes were cleaned and left in DW for 24 h at room temperature.

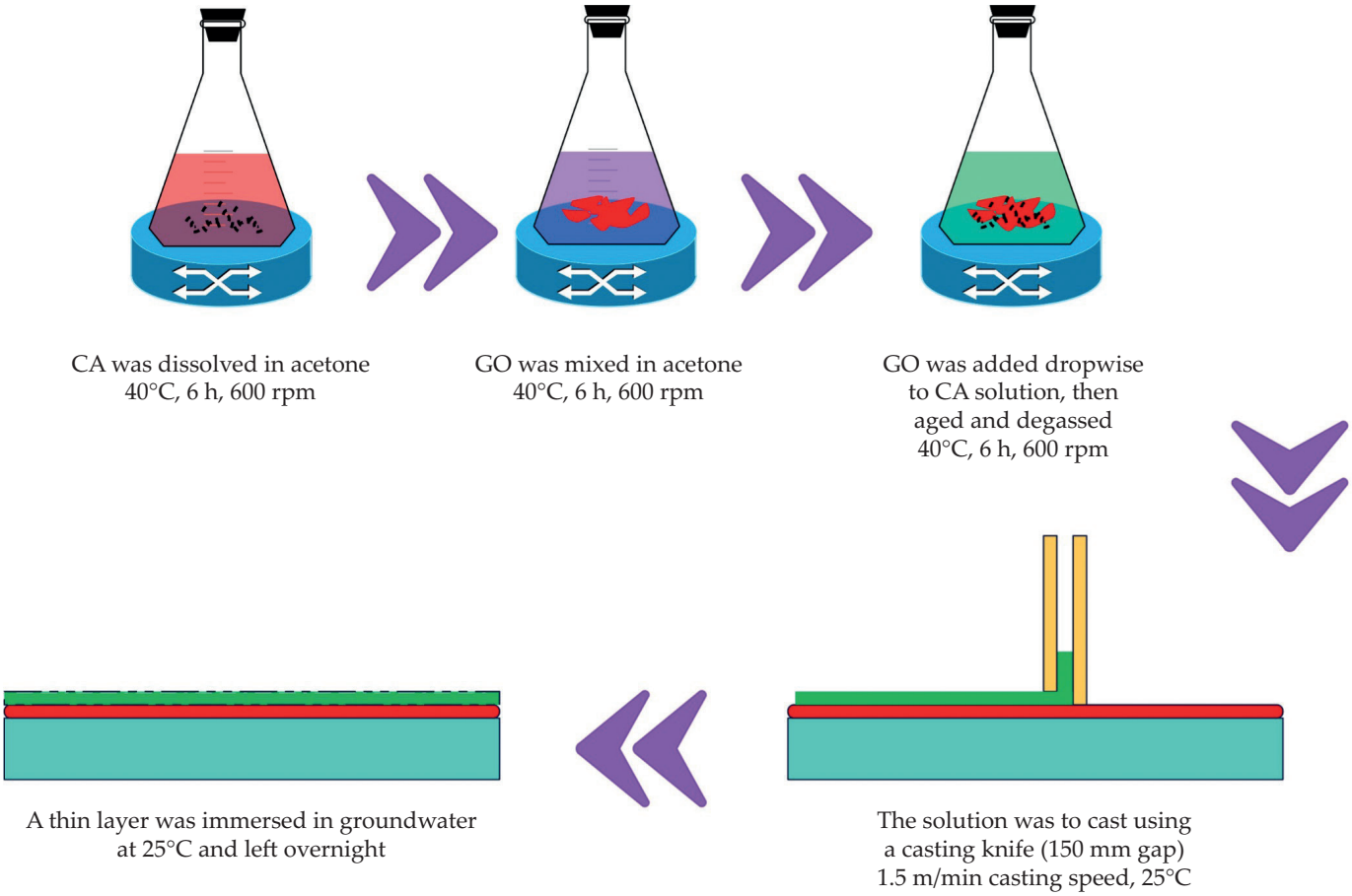

Fig. 1. Membranes preparation method

Characterization of membranes

Following membrane manufacturing and dead-end filtering, the membrane was subjected to Fourier transform infrared (FT-IR) spectroscopy and field emission scanning electron microscopy (FESEM) analyses to further understanding of the properties of the generated membranes. A Nicolet 6700 FT-IR spectrometer (Thermo Scientific, Waltham, MA, USA) was used, which covers the spectral range of 4000-280 cm^{-1}Before analysis, the membrane was attached to an aluminium sample holder using double-sided carbon tape. A LEO 1455 VP electron microscope (Zeiss, Oberkochen, Germany) was used to examine the morphology and structure of the membrane surface using an accelerating voltage of 20 kV. To reach a resolution of 3.5 nm, the device required 12 mA of current. The gravimetric approach that can be used to determine the total porosity (ε) is outlined in Equation 1:

$$\varepsilon = \frac{\omega_1 - \omega_2}{A \cdot l \cdot d_w} \quad (1)$$

Where: A – membrane surface area, l – membrane thickness, d_w – water density (998 kg/m^3), ω_1 and ω_2 – wet and dried membrane weights, respectively.

Equation 2 was used to determine the pore diameters of the manufactured membranes using the porosity data and the Guerout-Elford-Ferry equation (Equation 2).

$$r_m = \sqrt{\frac{(2.9 - 1.75\varepsilon)8\eta lQ}{\varepsilon \cdot A \cdot \Delta P}} \quad (2)$$

Where: Q – amount of pure water that permeates the membrane in a unit of time (m^3/s), ΔP – operational pressure (0.4MPa), η – water viscosity ($8.9 \cdot 10^{-4}$ Pa · s). The equipment used to measure the contact angle (CA) was the DSA1000 (Kruss Gmbh, Hamburg Germany).

A stainless-steel needle was used to inject the drips onto the membrane's surface. Before the analysis, all the membranes were allowed to air dry for a whole night at room temperature to remove the impact of capillary penetration. To reduce error in the progress, the contact angle test has been performed three times for each sample.

Membrane study

Membrane studies have been conducted to better understand membrane characteristics in the filtration process.

Membrane performance tests

The water flow through the membranes was measured using a mixing chamber. A fabricated flat membrane with an effective surface area of 10 cm^2, which

was embedded in CA/GO, was placed at the bottom of a Sterlitech HP4750 mixing chamber (Auburn, WA, USA). The membrane was compacted for 30 min at 2 bar using RO water to remove any remaining impurities and to obtain a more consistent solution flow. The membrane was supported by a porous plate. Equation 3 was then used to calculate the pure water flow through the membranes at different transmembrane pressures (1, 3 and 6 bar).

$$J = \frac{\Delta V}{A \cdot \Delta t} \tag{3}$$

Where: A – effective membrane surface area, Δt – filtration duration, J – the permeate flux, ΔV – the permeate cumulative volume.

Next, the gradient of the curve representing the membrane permeability was obtained by plotting the flow against pressure graph.

Fouling testing

A non-return filtration experiment was performed using a 200 mL mixing chamber. A 500 ppm Congo red dye solution was used for flow studies. A membrane sample with an effective area of 10 cm^2 was placed at the bottom of a SterlitechTM HP4750 (Auburn, WA, USA) mixing chamber and held in place by a porous plate. A 500-rpm single-blade mixer was also installed in the mixing chamber to reduce the formation of fouling layers at higher concentrations in the vicinity. The membrane was rinsed twice with clean water for approximately thirty seconds each time the test solution was removed after the filtration experiment at the operating pressure. Reusing RO water in the filtration experiment allowed for the measurement of the ultra-pure water flux across the same membrane. The calculation of membrane fouling resistances was based on the permeability of water passing through the membrane, as demonstrated by Equations 4 and 5.

$$J_{v1} = \frac{\Delta P}{\mu R_t} = \frac{\Delta P}{\mu (R_T)} \tag{4}$$

$$J_{v2} = \frac{\Delta P}{\mu R_t} = \frac{\Delta P}{\mu (R_m + R_f)} \tag{5}$$

Where: J_{v1} and J_{v2} – membrane permeate flux of pure and Congo red water, respectively; ΔP – transmembrane pressure, μ – water dynamic viscosity; R_m – membrane resistance; R_t – membrane resistance for clean water; R_f – fouling resistance.

Congo red's observed rejection was calculated using Equation 6.

$$R = 1 - \frac{c_p}{c_f} \tag{6}$$

Where: C_p and C_f – concentrations of the permeate and feed solutions, respectively.

RESULTS AND DISCUSSION

As can be seen in Figure 2, the addition of GO to CA did not significantly change the structure of any of the fabricated membranes, which, as shown by FESEM analysis, had a sponge-like structure. However, CA/GO membranes show significantly higher porosity compared to pure CA membrane, which is related to the addition of GO. GO promotes membrane permeability. The upper surface of the membrane shape develops into a thick, nonporous skin, as seen in Figure 2. This is since the interfacial polymer's concentration rises upon contact with the water bath, causing it to crystallize and immediately generate a skin densely packed with large crystal grains. For this type of membrane, the crystal formation for CA is well known and has been previously reported [32]. The surface shape of the membranes did not change significantly. There were no visible flaws or distortions on the membranes' surface. This is similar to how other polymer additives described in the literature work, with GOs playing a similar role in the formation of the porous structure of CA membranes during casting [33].

FT-IR spectroscopy was used to identify the functional groups in CA and composite membranes, as shown in Figure 3. Based on the FT-IR spectra, the vibrational frequencies of peaks for the CA and GO/CA samples are determined and shown in Table 1.

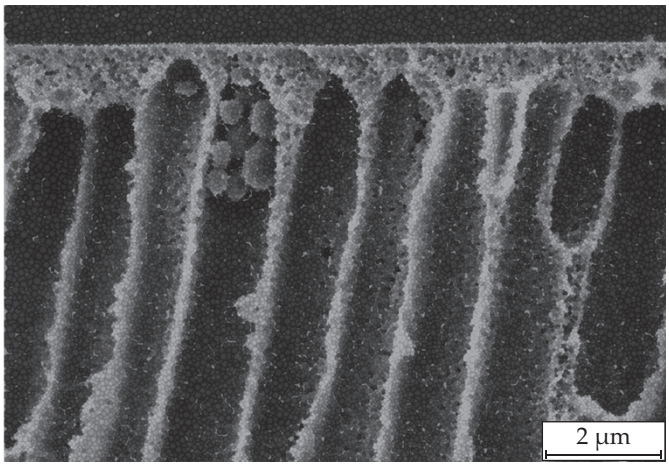

Fig. 2 FESEM image of CA membrane with 0.4 wt% GO

The molecular structure of CA was confirmed by FT-IR as shown in Figure 3. The characteristic bands of GO shift with increasing GO content toward lower or higher wavenumber values (± 5 cm^{-1}). Moreover, the intensity of the peaks originating from GO increases, confirming that the CA/GO composites were successfully formed.

The membrane's hydrophilicity can be determined by looking at its surface wettability. A more hydrophilic membrane surface is indicated by a lower pure water contact angle. As seen in Fig. 4, the addition of GO decreased the contact angle at the membrane surface. The pure water contact angle for the pure CA membrane was 55.47°. The water contact angle was 52.48° for 0.1 wt.% GO

T a b l e 1. Assignment of the bands in membranes FT-IR spectra

Wavenumber, cm^{-1}	Assignment
2912	C-H asymmetric stretching
1728	C-O-C asymmetric stretching
1598	H-C-H asymmetric stretching
1454	H-C-H deformation
1353	CH_2 deformation
1268	C-C-H symmetric bending
1096	C-C-H symmetric bending
795	C-C-H stretching
704	C-CH bending
377	O=C-H bending

content. This was explained by the fact that the mixed matrix membranes' interface energy was decreased by the functional groups of GO on the membrane surface [34]. It is commonly known that an increase in hydrophilicity has a direct effect on the flow of pure water. On the other hand, there was virtually a little pure-water flux in the membrane with 0.4 wt% GO. The increased viscosity of the blend solutions was responsible for the increase in hydrophilicity. The solution became more viscous and the mass transfer between the solvent and non-solvent phases was slowed down when high ratios of GO were added. When it comes to phase inversion events, this phenomenon is the main factor regulating the pore size of the manufactured membranes [35]. This feature can be explained by GO's amphiphilic nature, as seen by the relationship between the hydrophilic polysaccharide residues in GO and the hydrophobic Congo Red particles. This behaviour in GO has several applications, including stabilizing oil-water emulsions through the adsorption of GO's hydrophobic sites onto the surface of oil droplets, with its hydrophilic implications limiting droplet agglomeration and coalescence. The contact angle of CA/GO membranes is presented in Fig. 4. The amphiphilic nature of graphene oxide allows it to interact with both hydrophilic and hydrophobic elements, impacting the contact angle values shown in the figure. GO's oxygen-containing functional groups enable strong interactions with water (hydrophilicity), while its non-polar carbon regions can engage with hydrophobic surfaces. This dual nature contributes to the changes in wettability observed when GO is mixed with cellulose acetate. The contact angle decreases with the addition of 0.4 wt% GO, indicating enhanced hydrophilicity due to GO's amphiphilic interactions. However, a higher concentration (0.8 wt% GO) results in an increased contact angle, suggesting a complex balance between GO's hydrophilic and hydrophobic properties that alters surface characteristics [36].

Fouling testing

The life and separation efficiency of a membrane filtration system are determined by membrane fouling. The long-term performance of a good membrane can include high flux and low fouling tendency. The complex phenomenon known as membrane fouling can be caused by several factors, including concentration polarization, development of cake layers on the membrane surface, and plugging or clogging of membrane pores.

Hydrophilic surfaces are well known for their ability to draw in water molecules and create a layer of water. Figure 5 illustrates how water layer lessens the fouling tendency by delaying the absorption of Congo Red fouling agents. The contact angle decreasing of the membranes agrees with the trend of the flux recovery ratio. The CA/GO (99.2/0.8) membrane is an exception to this rule due to its larger pore radius, which could potentially allow Congo red to enter the pores and cause contamination. When GO was added to the CA casting solutions, it was found that the permeation flow increased in contrast to the pure CA membrane. Increases in the membranes' porosity, pore size, and hydrophilicity are the cause of the improved flow of the created membranes, which in result, raise permeability. When GO was added to the CA casting solutions, the penetration of CA membranes dramatically increased and exceeded the levels that had been described in the literature previously when specific additives were applied to the CA casting solutions

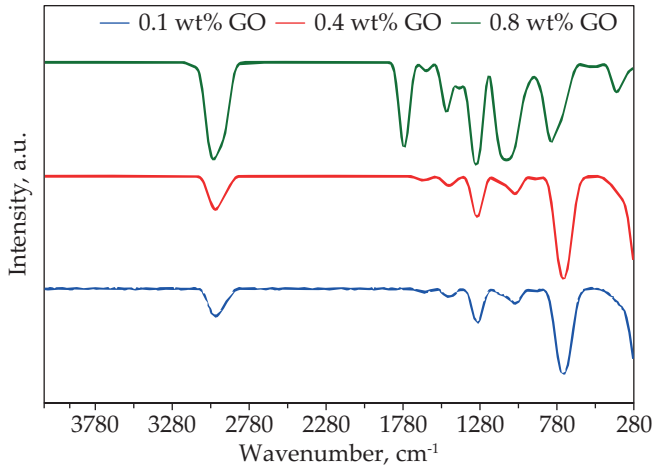

Fig. 3. FT-IR spectra of CA/GO membranes

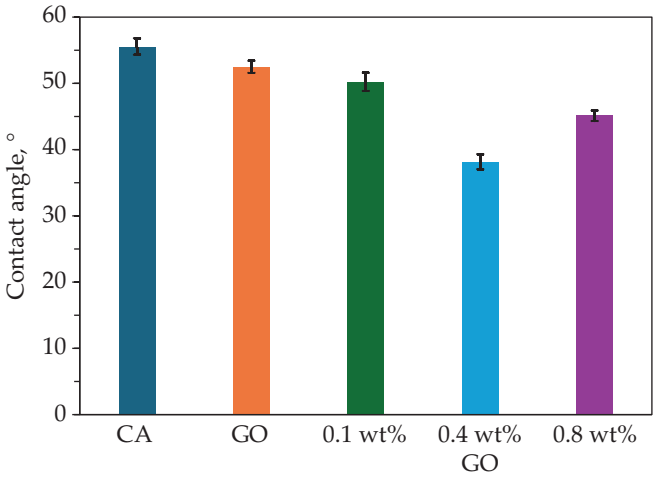

Fig. 4. The contact angle of CA, GO and CA/GO membranes

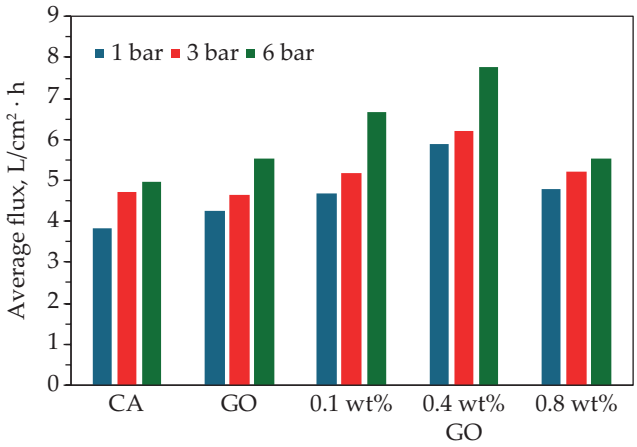

Fig. 5. Congo red contamination of the membrane at different pressures

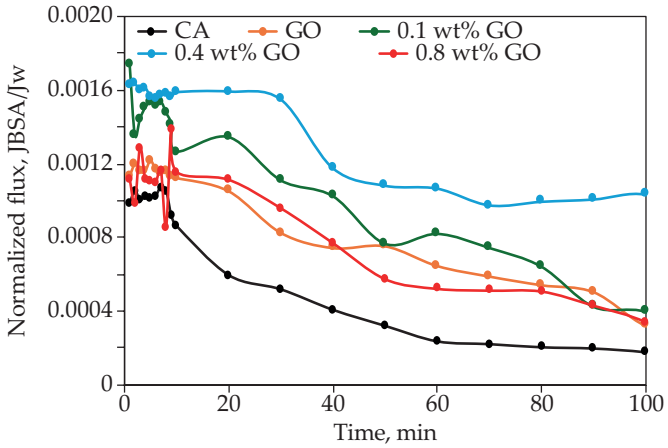

Fig. 6. The membranes contamination using Congo red

[37, 38]. Compared to pure membranes, these results demonstrated the modified membranes' exceptional antifouling capabilities. The CA/GO (99.6/0.4) membrane's irreversible fouling was lessened, indicating that reversible fouling predominated over all membrane fouling events for the changed membranes and that hydraulic cleaning would reverse the fouling impact [39-41].

Because GO has hydrophilic properties that will decrease the contact angle and increase the average flux, it is possible that this phenomenon was caused by the increased hydrophilicity of the membrane surface, which improved the antifouling properties by decreasing the absorption of Congo red or the build-up of foulants on the membranes. This indicates that the surface characteristics of the membrane and the overall qualities of the manufactured membranes were enhanced by the addition of graphene oxide to the membrane matrix. The contact angle measurements and these outcomes agree.

The hydrophobic nature of a membrane may be the source of poor antifouling property behaviour. Membrane fouling is always accompanied by both irreversible and reversible fouling. Firm Congo red molecule adsorption on the surface or entrapment of Congo red molecules in holes generate irreversible fouling, which is easily cleansed by hydraulic cleaning. Reversible fouling is caused by reversible Congo red adsorption. The results for BSA solution flow are shown in Fig. 6.

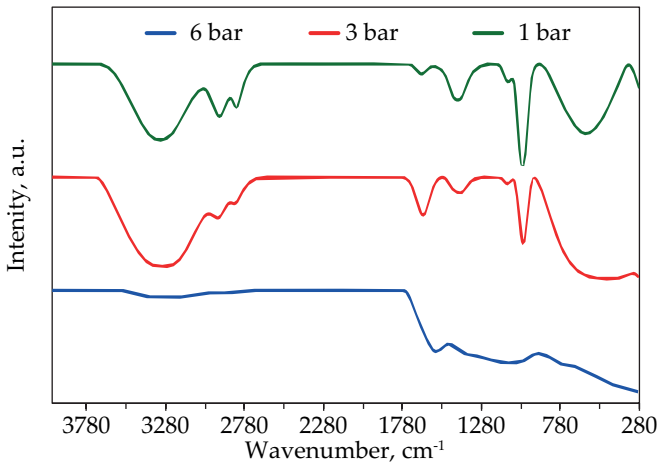

Fig. 7. FT-IR spectra of CA/GO (99.6/0.4) membrane after Congo red filtration at different pressures

Membrane stability

The results of the FT-IR research demonstrate that the FT-IR spectra of the new membranes with very little modifications are identical. According to the acquired FT-IR spectra (Fig. 7), the large peaks at around 3315 cm^{-1} are indicative of the stretching vibration of the C=O functional group and the deformation vibration of the O–H functional group, respectively. The stretching vibration for the C=O functional group is confirmed by the spikes at approximately 1642 cm^{-1}. The vibrational frequencies of the peaks in each sample are identified using the FT-IR spectra obtained for this study.

Comparison with other studies

The most appropriate cellulose derivative for electrospinning procedures is cellulose acetate (CA), which is created by esterifying cellulose using the esterification process [42]. Furthermore, it has antibacterial qualities and can be applied in a variety of biomedical fields. CA that has been electrospun is a biodegradable and biocompatible polymer with a high porosity content. It has a significant capacity for storing desired molecules because of its high surface-to-volume ratio. Because of this, there is a good chance that it will be used in applications including medicine administration and wound dressing. Because of its porosity and interconnected pores, CA has a higher surface-to-volume ratio, which makes it an excellent option for applications involving drug administration. Even though CA has a hydrophobic character due to the acetyl groups on its glucose units, these features make it a good substitute. It has been shown that GO is considered to be biocompatible with normal cells, which is consistent with the data in [43]. Due to its association with CA nanofiber, it is feasible to create textiles that can self-destruct. It is feasible to construct such textiles.

T a b l e 2. Comparison with other studies

Application	Nanocomposite	Effect	References
Drug delivery, wound healing, and tissue engineering	Ag and rGO-functionalized PU nanofibers	Bactericidal impact	[44]
Applications of antibacterial agents	Silver NP-doped graphene oxide/ peptide NFM	Antimicrobial properties	[45]
Protective clothing	ZnO nanorods with Ag nanoparticles adorn PMMA nanofibers	Photocatalytic, antiviral, and antibacterial properties	[46]
Body and health protection (excellent mechanical and sanitary parameters)	Elastic NFMs made of ZnO, CuO NPs, and thermoplastic TPU nanofibers	Antiviral and antimicrobial activity	[47]
Antibacterial coating substance to provide surfaces antibacterial action	NFM biopolymer graphene oxide-silver functionalized nanocomposites	Antimicrobial effect	[48]
Sports/outdoor textiles	PVA/zinc oxide NFMs	Antimicrobial activity	[49]
Water and air filters and wound dressings	Ag NPs embellished PET NFM.	Prevention of biofilms formation	[50]
Textiles for medicine	Cu-carbon nanoparticles with polyamide composite microfibers	Antifungal and antibacterial properties	[51]
Antibacterial coating substance providing surfaces with antibacterial properties	Biopolymer NFM functionalized with silver-graphene oxide nanocomposites	Antimicrobial effect	[48]
Packaging films, surgical dressings, and nonwoven textiles	Ag NPs embellished PVA NFM	Capacity to inhibit bacteria	[52]

CONCLUSIONS

In this study, the methods for improving the overall membrane properties and reducing fouling were investigated. In the membrane production process, CA-coated graphene oxide proved to be an effective new nano-filler. Mixed-matrix membranes manufactured from graphene oxide are very promising for large-scale industrial membrane production. However, problems in the graphene oxide production process make it less suitable for membrane modification. Therefore, the main objective of this work was to modify the properties of graphene oxide to improve the overall membrane performance. The resulting membranes exhibited high hydrophilicity. The contact angle was reduced from 55.47° to 38.16°, which improved the flow and fouling resistance, respectively. Future work should focus on enhancing the long-term stability and scalability of GO-modified membranes for industrial applications. It is crucial to address challenges in the production process of graphene oxide, such as improving its structural stability and ensuring uniform dispersion in the membrane matrix. Potential improvements may include functionalizing GO with other nanomaterials or polymers to enhance durability and prevent degradation. In addition, optimizing fabrication methods to achieve consistent membrane performance and cost-effective large-scale production will be essential for successful industrial implementation.

Authors contribution

M.J. – conceptualization, methodology, validation, investigation, writing-original draft, writing-review and editing, visualization; H.A.M. – methodology, validation, writing-review and editing; A.A.H. – methodology, conceptualization, supervision; M.A.I. – conceptualization, supervision; A.G.T. – conceptualization, supervision; M.A.N. – conceptualization, supervision.

Funding

This research received no external funding.

Conflict of interest

The authors declare that they have no known competing financial interests or personal relationships that could have appeared to influence the work reported in this paper.

REFERENCES

[1] Almanassra I.W., Jaber L., Manawi Y. *et al.*: *Chemical Engineering Journal* **2024**, *488*, 151029. https://doi.org/10.1016/j.cej.2024.151029

[2] Li Z., Chen M., Zhu W. *et al.*: *Coordination Chemistry Reviews* **2024**, *520*, 216124.

https://doi.org/10.1016/j.ccr.2024.216124
[3] Farooq N., ur Rehman Z., Hareem A. *et al*.: *MatSci Express* **2024**, *1(4)*, 185.
[4] Avornyo A., Chrysikopoulos C.V.: *Journal of Environmental Management* **2024**, *353*, 120178. https://doi.org/10.1016/j.jenvman.2024.120178
[5] Vafa N., Firoozabadi B., Pishkenari H.N.: *Journal of Molecular Liquids* **2024**, *407*, 125241. https://doi.org/10.1016/j.molliq.2024.125241
[6] Cano F.J., Coste S., Reyes-Vallejo O. *et al*.: *Surfaces and Interfaces* **2024**, *46*, 104004. https://doi.org/10.1016/j.surfin.2024.104004
[7] Guo L., Wen Y., Li F. *et al*.: *Suraces and Interfaces* **2024**, *51*, 104727. https://doi.org/10.1016/j.surfin.2024.104727
[8] Moriyama N., Takenaka R., Nagasawa H. *et al*.: *ACS Applied Materials and Interfaces* **2024**, *16(6)*, 8086. https://doi.org/10.1021/acsami.3c16844
[9] Azrak V., Öter Ö., Oğuzlar S. *et al*.: *Journal of Materials Science: Materials in Electronics* **2024**, *35*, 1679. https://doi.org/10.1007/s10854-024-13455-x
[10] Fonsaca J.E.S., Lima C.E., Martins K.S.B. *et al*.: *Langmuir* **2024**, *40(41)*, 21442. https://doi.org/10.1021/acs.langmuir.4c02235
[11] Lin T., Wen X., Ren X. *et al*.: *Small Structures* **2024**, 2400320. https://doi.org/10.1002/sstr.202400320
[12] Vo T.S., Lwin K.M., Kim K.: *Advanced Composites and Hybrid Materials* **2024**, *7*, 127. https://doi.org/10.1007/s42114-024-00923-5
[13] Wang Y., Zhang Y., Zuo H. *et al*.: *Desalination* **2024**, *587*, 117933. https://doi.org/10.1016/j.desal.2024.117933
[14] Dai J., Li L., Fang Q. *et al*.: *Chemical Engineering Journal* **2024**, *495*, 153355. https://doi.org/10.1016/j.cej.2024.153355
[15] Thangarasu S., Palanisamy G., Sadhasivam S. *et al*.: *Journal of Materials Chemistry A* **2024**, *12*, 11176. https://doi.org/10.1039/D4TA00001C
[16] Manobalan S., Sumangala.: "MXene-Based Polymer Composite Membranes for Pervaporation and Gas Separation" in "MXene Reinforced Polymer Composites: Fabrication, Characterization and Applications", (editors: Deshmukh K., Pandey M., Hussain C.M.), Scivener Publishing, Beverly 2024). p. 501. https://doi.org/10.1002/9781119901280.ch15
[17] Azadi E., Singh N., Dinari M. *et al*.: *Chemical Communications* **2024**, *60*, 2865. https://doi.org/10.1039/D3CC06057H
[18] Feng F., Yang Y., Liu Q. *et al*.: *Journal of Hazardous Materials* **2024**, *476*, 134952. https://doi.org/10.1016/j.jhazmat.2024.134952
[19] Ibrahim G.M., Alshahrani S.M., Alosaimi E.H. *et al*.: *Journal of Molecular Structure* **2024**, *1298 (Part 1)*, 136992. https://doi.org/10.1016/j.molstruc.2023.136992
[20] Kang Y., Xia Y., Wang H. *et al*.: *Advanced Functional Materials* **2019**, *29(29)*, 1902014. https://doi.org/10.1002/adfm.201902014
[21] Xing Y.L., Xu G.R., An Z.H. *et al*.: *Separation and Purification Technology* **2021**, *259*, 118192. https://doi.org/10.1016/j.seppur.2020.118192
[22] Cheng L., Liu G., Zhao J. *et al*.: *Accounts of Materials Research* **2021**, *2(2)*, 114. https://doi.org/10.1021/accountsmr.0c00092
[23] Abdulkareem-Alsultan G., Asikin-Mijan N., Obeas L.K. *et al*.: *Chemical Engineering Journal* **2022**, 429, 132206. https://doi.org/10.1016/j.cej.2021.132206
[24] Wang X., Mao Y.F., Shen X. *et al*.: *Separation and Purification Technology* **2024**, *329*, 125216. https://doi.org/10.1016/j.seppur.2023.125216
[25] Sun Z., Kong P., Gui H. *et al*.: *Materials Today Chemistry* **2024**, *41*, 102303. https://doi.org/10.1016/j.mtchem.2024.102303
[26] Kamil F.H., Salmiaton A., Shahruzzaman R.M.H.R. *et al*.: *Bulletin of Chemical Reaction Engineering and Catalysis* **2017**, *12(1)*, 81. https://doi.org/10.9767/bcrec.12.1.557.81-88
[27] Thebo K.H., Qian X., Zhang Q. *et al*.: *Nature Communications* **2018**, *9(1)*, 1486. https://doi.org/10.1038/s41467-018-03919-0
[28] Alsultan A.G., Asikin Mijan N., Mansir N. *et al*.: *ACS Omega* **2021**, *6(1)*, 408. https://doi.org/10.1021/acsomega.0c04800
[29] Lv X.B., Xie R., Ji J.Y. *et al*.: *Separation and Purification Technology* **2024**, *336*, 126232. https://doi.org/10.1016/j.seppur.2023.126232
[30] Wang Y., Ren L., Wang H. *et al*.: *Chemical Engineering Journal* **2024**, *485*, 149742. https://doi.org/10.1016/j.cej.2024.149742
[31] Abdulkreem-Alsultan G., Islam A., Janaun J. *et al*.: *Materials Letters* **2016**, *179*, 57. https://doi.org/10.1016/j.matlet.2016.05.030
[32] Qin K., Zheng Z., Wang *et al*.: *Giant* **2024**, *19*, 100317. https://doi.org/10.1016/j.giant.2024.100317
[33] Oberlintner A., Shvalya V., Santhosh N.M. *et al*.: *Carbohydrate Polymers* **2024**, *345*, 122558. https://doi.org/10.1016/j.carbpol.2024.122558
[34] Abdalla O., Rehman A., Nabeeh A. *et al*.: *Membranes* **2023**, *13(7)*, 678. https://doi.org/10.3390/membranes13070678
[35] Macedonio F., Alessandro F., Frappa M. *et al*.: "New applications of polymeric phase inversion membranes" in "Polymeric Membrane Formation by Phase Inversion", (editors: Tavajohi N., Khayet M.), Elsevier, Amsterdam 2024. p. 395. https://doi.org/10.1016/B978-0-323-95628-4.00017-3
[36] Ghassan A.A., Mijan N.A., Taufiq-Yap Y.H.: "Nanomaterials: An Overview of Nanorods Synthesis and Optimization" in "Nanorods and Nanocomposites", (editors: Ghamsari M.S., Dhara S.), Intertech Open, London 2020, p. 11.

[37] Raja R.I., Rashid K.T., Toma M.A. *et al*.: *Journal of Saudi Chemical Society* **2024**, *28(2)*, 101805. https://doi.org/10.1016/j.jscs.2023.101805
[38] Lum M.M.X., Ng K.H., Lai S.Y. *et al*.: *Process Safety and Environmental Protection* **2023**, *176*, 580. https://doi.org/10.1016/j.psep.2023.06.035
[39] Liu L., Wang Y., Liu Y. *et al*.: *Environmental Pollution* **2024**, *347*, 123750. https://doi.org/10.1016/j.envpol.2024.123750
[40] Mansir N., Sidek H.M., Teo S.H. *et al*.: *Bioresource Technology Reports* **2022**, *17*, 100988. https://doi.org/10.1016/j.biteb.2022.100988
[41] Elouahed S.K., Asikin-Mijan N., Alsultan A.G. *et al*.: *Energy Conversion and Management* **2024**, *303*, 118185. https://doi.org/10.1016/j.enconman.2024.118185
[42] Shakhabutdinov S.S., Yugay S.M., Ashurov N.S. *et al*.: *Eurasian Journal of Chemistry* **2024**, *49(2)*, 21. https://doi.org/10.31489/2959-0663/2-24-2
[43] Mateu-Sanz M., Fuenteslópez C.V., Uribe-Gomez J. *et al*.: *Trends in Biotechnology* **2024**, *42(4)*, 402. https://doi.org/10.1016/j.tibtech.2023.09.015
[44] Pant B., Park M., Jang R.S. *et al*.: *Carbon Letters* **2017**, *23*, 17. https://doi.org/10.5714/CL.2017.23.017
[45] He P., Yang M., Lei Y. *et al*.: *Polymers* **2023**, *15(5)*, 1321. https://doi.org/10.3390/polym15051321
[46] Karagoz S., Kiremitler N.B., Sarp G. *et al*.: *ACS Applied Materials and Interfaces* **2021**, *13(4)*, 5678. https://doi.org/10.1021/acsami.0c15606
[47] Alshabanah L.A., Omran N., Elwakil B.H. *et al*.: *Polymers* **2021**, *13(22)*, 2987. https://doi.org/10.3390/polym13223987
[48] de Faria A.F., Perreault F., Shaulsky E. *et al*.: *ACS Applied Materials and Interfaces* **2015**, *7(23)*, 12751. https://doi.org/10.1021/acsami.5b01639
[49] Lee K., Lee S.: *Textile Research Journal* **2015**, *85(19)*, 1999. https://doi.org/10.1177/0040517515578325
[50] Soltanolzakerin-Sorkhabi T., Fallahi-Samberan M., Kumaravel V.: *Molecules* **2023**, *28(14)*, 5439. https://doi.org/10.3390/molecules28145439
[51] Jin L., Zhou F., Wu S. *et al*.: *Textile Research Journal* **2022**, *91(1-2)*, 3. https://doi.org/10.1177/0040517521993484
[52] Yang Y., Zhang Z., Wan M. *et al*.: *Polymers* **2020**, *12(11)*, 2486. https://doi.org/10.3390/polym12112486

Received 29 VIII 2024.
Accepted 16 IX 2024

.